Pressure-induced deconfinement of the charge transport in the quasi-one-dimensional Mott insulator $(TMTTF)_2AsF_6$

A. Pashkin,* M. Dressel, and C. A. Kuntscher*,†
1. Physikalisches Institut, Universität Stuttgart, D-70550 Stuttgart, Germany
(Received 26 April 2006; published 27 October 2006)

We studied the pressure dependence of the room-temperature infrared reflectivity of $(TMTTF)_2AsF_6$ along all three optical axes. This anisotropic organic compound consists of molecular stacks with orbital overlap along the *a* direction; due to electronic correlations the system is a quasi-one-dimensional Mott insulator with a charge gap $\Delta_\rho \approx 70$ meV. The gap is gradually reduced with increasing external pressure, accompanied by the onset of a Drude contribution along the stacking direction. In the perpendicular *b'* direction a Drude-like optical response is observed for pressures above 2 GPa. This behavior is interpreted in terms of a deconfinement of the electrons in a one-dimensional Mott insulator, i.e., an insulator-to-metal transition which occurs when the interchain transfer integral t_b is approximately equal to half of the charge gap energy. We estimate the values of t_b and the Luttinger liquid parameter K_ρ as a function of pressure.

DOI: 10.1103/PhysRevB.74.165118 PACS number(s): 71.30.+h, 78.30.Jw, 62.50.+p

I. INTRODUCTION

The properties of quasi-one-dimensional conductors have been the subject of intensive studies for half a century. A theory based on the one-dimensional (1D) Hubbard model predicts a non-Fermi-liquid metallic state.[1–3] The situation, however, develops differently when the filling of the system is commensurate, since in this case, electronic interactions may cause a Mott insulating state. Although this phenomenon is possible in all dimensions, it is particularly strong in the 1D case via the umklapp process.[4] The influence of the interchain coupling on the electronic properties of a half- and quarter-filled quasi-1D interacting electron system was studied theoretically.[3,5–10] It is predicted[3,9] that with increasing interchain transfer integral $t_\perp$ such a system undergoes a deconfinement transition into a metallic state. The schematic phase diagram illustrating this phenomenon is shown in Fig. 1. Strictly speaking, the deconfinement transition takes place at $T=0$ when $t_\perp$ becomes larger than a certain value $t_\perp^*$ and can be referred to as a quantum phase transition. For $t_\perp < t_\perp^*$ the system is in a Mott insulating state and the single-particle interchain hopping is completely suppressed. If the interchain transfer integral exceeds a critical value $t_\perp^*$, the insulating state is broken and single-particle interchain hopping becomes possible. Thus the system evolves from a 1D Mott-Hubbard insulator to a high-dimensional metallic state (trajectory 1 in Fig. 1). The theoretical study[5,6] of two coupled Hubbard chains predicts a close relation of the interchain transfer integral to the charge gap, $t_\perp^* \propto \Delta_\rho$.[11] While in a simple two-chain system no real deconfinement is observed,[10] for a large (infinite) number of chains[12] the crossover is expected at some critical value $t_\perp^* \approx \Delta_\rho/2$.[5,13]

If the temperature or energy scale at which the response of the system is probed becomes larger than $t_\perp$, the warping of the open Fermi surface is masked. Therefore the properties of the system are virtually the same as in the case of a flat Fermi surface, i.e., for a strictly 1D system where the interacting electrons are described by the Luttinger liquid (LL) model.[1] Thus the deconfinement transition at high enough temperature leads to a crossover from a Mott insulating to a LL metallic state (see trajectories 2 and 4 in Fig. 1). Furthermore, a dimensional crossover from a LL to a high-dimensional metallic state occurs when the interchain coupling (i.e., the warping of the Fermi surface) becomes larger than the energy of thermal fluctuations ($t_\perp > k_B T$). This can be achieved by increasing the transfer integral $t_\perp$ (trajectory 3) or by lowering the temperature (trajectory 5). In the high-dimensional metallic state the Fermi-liquid description is valid instead of the LL model.

Suitable systems to study the predicted dimensional crossover and deconfinement transition are the well-known organic Bechgaard-Fabre salts[14–16] $(TMTTF)_2X$ and $(TMTSF)_2X$. They consist of weakly coupled molecular stacks along which the charge transport occurs. Hereby, the type of the molecule (TMTSF or TMTTF) and of the anions X^- determine the coupling between the molecular stacks and

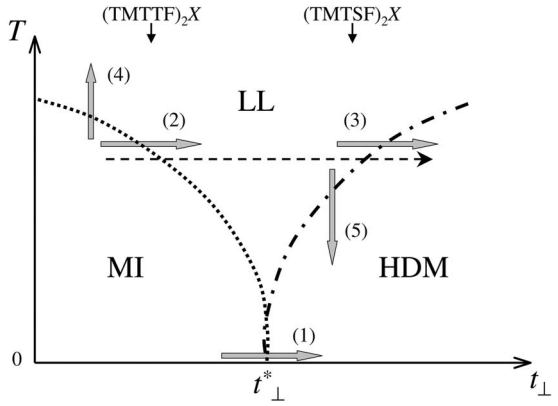

FIG. 1. Schematic phase diagram of the deconfinement transition for a system of weakly coupled conducting chains according to Refs. 3 and 9. Transition from a Mott insulator (MI) to a high-dimensional metallic (HDM) state occurs at $T=0$ when $t_\perp$ reaches a critical value $t_\perp^*$ (trajectory 1). At high enough temperature, the increase of $t_\perp$ leads to a transition from a Mott insulating to a 1D Luttinger liquid (LL) conducting state (trajectory 2) and finally to a dimensional crossover into an HDM state (trajectory 3). The temperature change at a fixed value $t_\perp$ may also lead to a transition from a Mott insulating to a LL state (trajectory 4), or to a dimensional crossover (trajectory 5). The horizontal dashed line indicates the path of our pressure study.

thus the dimensionality of the system (chemical pressure effect). In particular, the $(TMTTF)_2X$ salts consist of basically uncoupled chains, which are half-filled due to the dimerization along the chains. Thus they constitute systems of electrons confined to the chains, forming a Mott insulating state, and are located on the left side of the diagram given in Fig. 1. At low temperatures the Mott insulating state of $(TMTTF)_2X$ salts is transformed into a charge-ordered state characterized by a disproportion of charge of the donor TMTTF molecules within the stacks. This ferroelectric transition is strongly pressure-dependent, and the charge-ordered phase can be suppressed by the application of a moderate pressure of a few kbars.[17,18] On the other hand, the compounds $(TMTSF)_2X$ represent examples of quasi-1D metals and they are on the right side of the diagram, since the enhanced interchain coupling leads to a charge deconfinement.

The low-temperature optical conductivity spectra of the TMTSF salts along the stacks are characterized by two distinct features: a narrow mode at zero energy containing a very small part of the spectral weight and a high-energy mode centered at around 200 cm^{-1}.[19] The latter feature was interpreted in terms of the Mott (charge) gap of a 1D insulator.[20] The frequency dependence of the optical conductivity in the energy range above the effective interchain transfer integral [about 250 cm^{-1} for $(TMTSF)_2PF_6$] is well-described by a LL model, since the system can be considered as effectively one-dimensional. On the other hand, the zero-energy mode was suggested to originate from the effective doping of the 1D Mott insulator due to the deconfined interchain electron hopping. Thus it is related to 2D physics and could be successfully described by the Fermi-liquid model.[19] Similar on-chain optical conductivity spectra with the dominating Mott gap were also observed for TMTTF compounds.[21] However, the zero-energy mode typical for TMTSF salts is absent, since these systems are in the confined state where interchain hopping is suppressed. Thus optical spectroscopy on the high-energy range (larger than the interchain transfer integral) addresses electronic interactions in 1D, while dc resistivity measurements are more susceptible to interchain hopping and thus reveal deviations from a strictly 1D picture.

First hints for the deconfinement transition and the dimensional crossover were found by pressure-dependent transport measurements on $(TMTTF)_2PF_6$ and $(TMTSF)_2PF_6$ crystals.[22] The effect of the dimensional crossover occurring during the temperature decrease was addressed by an optical study of $(TMTSF)_2PF_6$.[23] Later on, the above-mentioned theoretical criterium for the deconfinement transition was verified by comparing the ambient-pressure optical spectra of different Bechgaard-Fabre salts,[13] i.e., making use of the effect of chemical pressure on the interchain coupling. However, this approach has disadvantages, since only a limited number of discrete pressure points corresponding to particular compounds are available. Moreover, atomic substitution (especially for sulfur and selenium atoms) may appreciably affect not only the interchain transfer integral $t_\perp$, but also the stack dimerization, on-chain bandwidth, Coulomb repulsion, etc.

A more direct and cleaner way to study the deconfinement transition experimentally is the application of external pressure, since the changes in the electrodynamic response can be monitored while the interchain coupling is being continuously tuned. In this paper we present the results of a pressure-dependent infrared spectroscopic study on the salt $(TMTTF)_2AsF_6$ which is a prime example of a 1D Mott-Hubbard insulator at ambient pressure.[17,22,24] The main aim of the present investigation is to determine the pressure-induced changes in the optical response of $(TMTTF)_2AsF_6$ during the deconfinement transition and the dimensional crossover. During our experiment we thus intended to follow the evolution of the system along the dashed arrow in Fig. 1. A quantitative analysis of the measured spectra was performed in order to extract the value of the interchain transfer integral $t_\perp$ as a function of pressure. The obtained results are compared to the ambient-pressure optical response of different Bechgaard-Fabre salts and discussed in terms of the expected crossover from insulating $(TMTTF)_2X$ to metallic $(TMTSF)_2X$ compounds.

II. EXPERIMENT

Single crystals of $(TMTTF)_2AsF_6$ were grown by standard electrochemical growth procedure. A diamond anvil cell equipped with type IIA diamonds suitable for infrared measurements was used to generate pressures up to 6 GPa. Finely ground CsI powder was chosen as the quasihydrostatic pressure transmitting medium. The measured samples had as-grown specular surfaces and a thickness of about 50 μm. The lateral dimensions were approximately 80×80 μm^2. The pressure in the cell was measured using the ruby luminescence method.[25] Polarized reflectivity spectra were recorded at room temperature utilizing a Bruker IFS 66v/S Fourier-transform-IR spectrometer in the midinfrared (mid-IR) frequency range (550–8000 cm^{-1}). To focus the beam on the small sample in the pressure cell, an infrared microscope (Bruker IRscope II) coupled to the spectrometer was used.

The intensity spectrum $I_d(\omega)$ reflected from the lower air-diamond interface of the diamond anvil served as reference. The obtained reflectivity spectra $R_{s\text{-}d}(\omega)$ refer to the absolute reflectivity at the sample-diamond interface calculated according to

$$R_{s\text{-}d}(\omega) = R_{dia}\frac{I_{s\text{-}d}(\omega)}{I_d(\omega)}, \tag{1}$$

where $I_{s\text{-}d}$ is the intensity reflected from the sample-diamond interface and R_{dia} is the absolute reflectivity of the diamond-air interface. Since the refractive index of diamond[26] $n_d = 2.38$ is almost frequency independent below 10^4 cm^{-1}, $R_{dia} \simeq 0.167$ was used in our analysis. Furthermore, it was assumed to be pressure-independent.[27] The reflectivity spectra $R_{s\text{-}d}(\omega)$ in the frequency range 1700–2700 cm^{-1} are affected by multiphonon absorptions of diamond, which cannot be perfectly compensated. Therefore this part of the measured spectra is not shown. In order to check the reproducibility of the results, we have performed four high-pressure measurements on different $(TMTTF)_2AsF_6$ crystals.

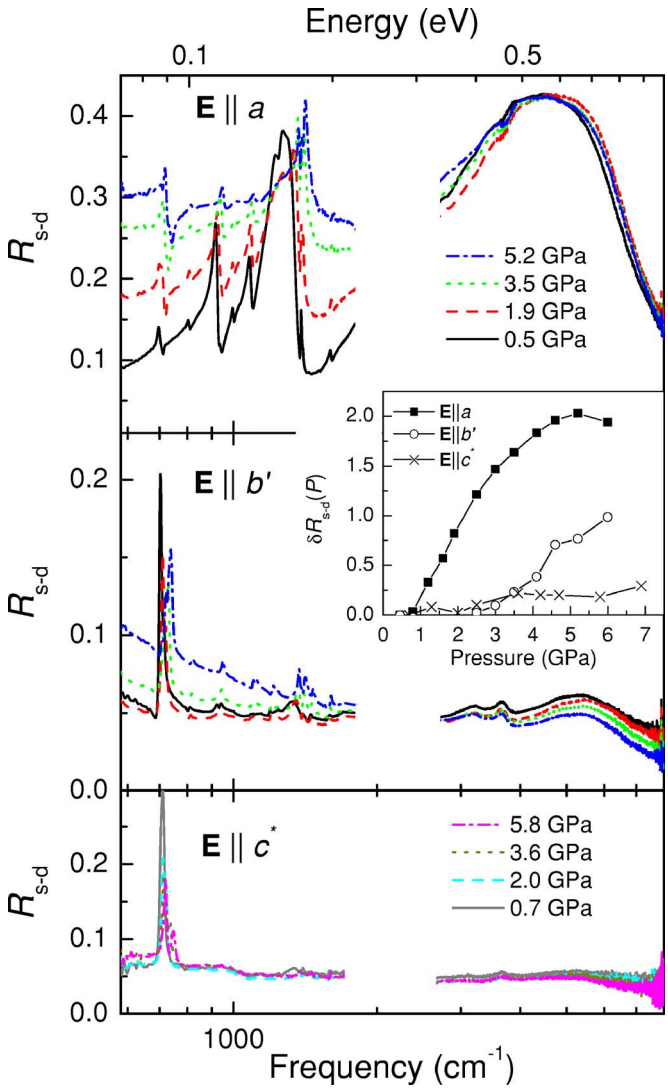

FIG. 2. (Color online) Room temperature reflectivity spectra $R_{s\text{-}d}$ of $(TMTTF)_2AsF_6$ as a function of pressure for $\mathbf{E}\|a$, $\mathbf{E}\|b'$, and $\mathbf{E}\|c^*$. Note the different pressure values for $\mathbf{E}\|a$, b', and $\mathbf{E}\|c^*$. The inset shows the normalized pressure-induced change of the reflectivity $\delta R_{s\text{-}d}(P)=R_{s\text{-}d}(P)/R_{s\text{-}d}(P_{\min})-1$ at 630 cm^{-1}.

III. RESULTS

Pressure-dependent reflectivity spectra are presented in Fig. 2 for the polarizations $\mathbf{E}\|a$ (stacking direction), $\mathbf{E}\|b'$ (direction perpendicular to a, in the $a-b$ plane), and $\mathbf{E}\|c^*$ (perpendicular to a and b'). Since the spectra for $\mathbf{E}\|c^*$ were obtained in a separate experimental run, the pressure values are slightly different from those for $\mathbf{E}\|a,b'$.

The $\mathbf{E}\|a$ reflectivity spectra include a strong mid-IR band at around 4600 cm^{-1} and a number of sharp vibrational modes below 2000 cm^{-1}. Most of them are totally symmetric electron-molecular-vibration (emv) coupled A_g Raman modes of the TMTTF molecule.[28] The application of pressure leads to the gradual increase of the low-frequency part (<2000 cm^{-1}) of the reflectivity. At the same time, the reflectivity level of the mid-IR band remains almost constant in the whole studied pressure range.

For $\mathbf{E}\|b'$ the reflectivity level is almost frequency-independent at low pressures (<2 GPa), except for the broad mid-IR absorption band located at around 5300 cm^{-1}. The sharp peak at around 700 cm^{-1} is related to the F_{1u} symmetry vibration of the octahedral AsF_6 anion.[29] Other weaker vibrational features for $\mathbf{E}\|b'$ can be assigned to the B_{1u} and B_{2u} IR-active modes of the TMTTF molecules.[30] The application of high enough pressure (>2 GPa) results in a pronounced increase of the reflectivity in the low-frequency range (<2000 cm^{-1}). At the same time, the intensity of the mid-IR band decreases, while its frequency position remains almost unchanged. In contrast to the other studied directions, the reflectivity for $\mathbf{E}\|c^*$ is very low, almost frequency-independent (except for the sharp AsF_6 vibration at 700 cm^{-1}), and does not change with the application of pressure up to 6 GPa.

The value of the low-frequency reflectivity (<2000 cm^{-1}) is mostly affected by the Drude contribution due to free electrons. Therefore the pressure-induced enhancement of the charge transport should lead to a higher reflectivity at low frequencies. This is illustrated in the inset of Fig. 2, where the change of the reflectivity $\delta R_{s\text{-}d}(P)=R_{s\text{-}d}(P)/R_{s\text{-}d}(P_{\min})-1$ at 630 cm^{-1} normalized to the reflectivity at the lowest applied pressure $P_{\min}$ is depicted as a function of applied pressure P. The enhancement of the reflectivity along the stacks ($\mathbf{E}\|a$) is as large as a factor of 2 at 5.2 GPa. For $\mathbf{E}\|b'$ the increase becomes noticeable only above 3 GPa, and reaches one at the highest applied pressure. In contrast, the spectra of $\mathbf{E}\|c^*$ show a very small increase of only ≈ 0.2 at 6 GPa, which cannot be analyzed quantitatively.

IV. ANALYSIS AND DISCUSSION

A. Longitudinal optical response

In order to extract the optical conductivity for $\mathbf{E}\|a$ from the measured pressure-dependent reflectivity spectra, we have carried out a Kramers-Kronig (KK) analysis. The application of this method to our data is not trivial due to two reasons: (i) The measured reflectivity spectra cover a limited frequency range; for the KK analysis they need to be extrapolated to lower and higher frequencies and interpolated within the diamond absorption range (1700–2700 cm^{-1}). (ii) The standard KK relation between the reflectivity and phase needs to be corrected when it is applied to the sample-diamond interface, $R_{s\text{-}d}$, and the necessary correction term contains an *a priori* unknown parameter.[31]

As a first step in the analysis of the reflectivity data $R_{s\text{-}d}(\omega)$, we performed an approximate fitting of the reflectivity data. Most of the observed phonon resonances are characterized by an asymmetric line shape and cannot be fitted by a simple three-parameter Lorentz model. We therefore used an extended four-parameter factorized oscillator model[32] for the fitting, which is frequently applied for the analysis of IR phonon modes. The dielectric function in this model is described by

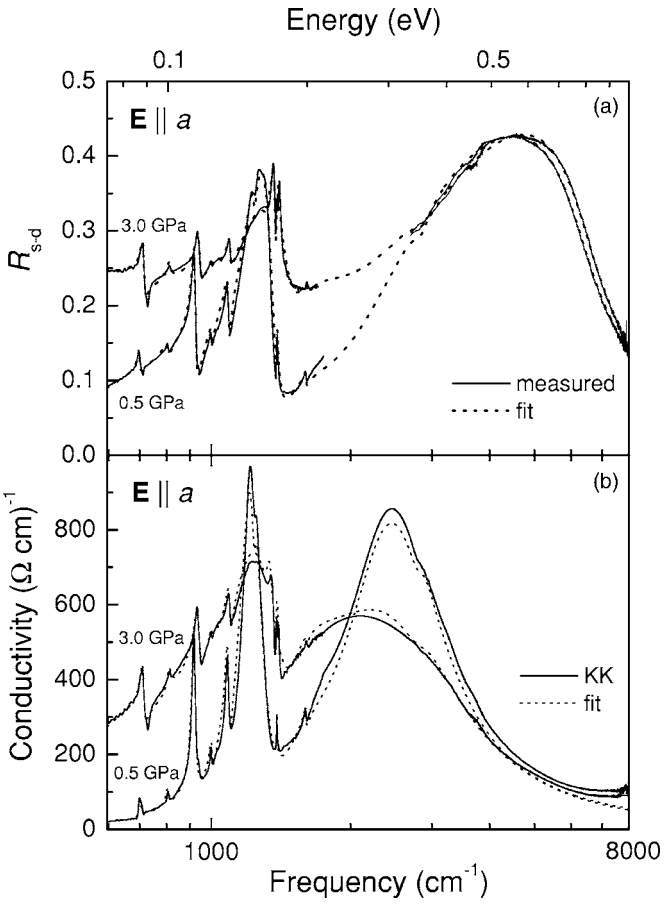

FIG. 3. (a) Comparison of the measured reflectivity $R_{s\text{-}d}$ of $(TMTTF)_2AsF_6$ with the fits, according to Eqs. (2) and (3), for $\mathbf{E}\|a$ for two pressures (0.5 and 3.0 GPa). (b) Corresponding optical conductivity $\sigma_1(\omega)$ spectra from the fit compared with the optical conductivity obtained by the KK analysis.

$$\epsilon(\omega) = \epsilon_\infty \prod_{j=1}^{n} \frac{\omega_{LO_j}^2 - \omega^2 + i\omega\gamma_{LO_j}}{\omega_{TO_j}^2 - \omega^2 + i\omega\gamma_{TO_j}}, \tag{2}$$

where ω_{TO_j} and ω_{LO_j} are transverse and longitudinal frequencies of the jth polar mode, respectively, γ_{TO_j} and γ_{LO_j} their respective damping constants, and ϵ_∞ the optical dielectric constant far above the resonance frequencies. The reflectivity is then calculated according to

$$R_{s\text{-}d} = \left| \frac{\sqrt{\epsilon(\omega)} - n_d}{\sqrt{\epsilon(\omega)} + n_d} \right|^2. \tag{3}$$

With this procedure we were able to fit the measured reflectivity spectra rather precisely. As examples, we show the results of the fits together with the measured spectra for two pressures (0.5 and 3 GPa) in Fig. 3(a).

The obtained fits were used for the extrapolation of the experimental spectra to lower and higher frequencies necessary for the KK analysis. The reflectivity in the diamond absorption range (1700–2700 cm^{-1}) was linearly interpolated. The KK relation for the phase of the reflectivity $R_{s\text{-}d}$ has the following form:[31,33]

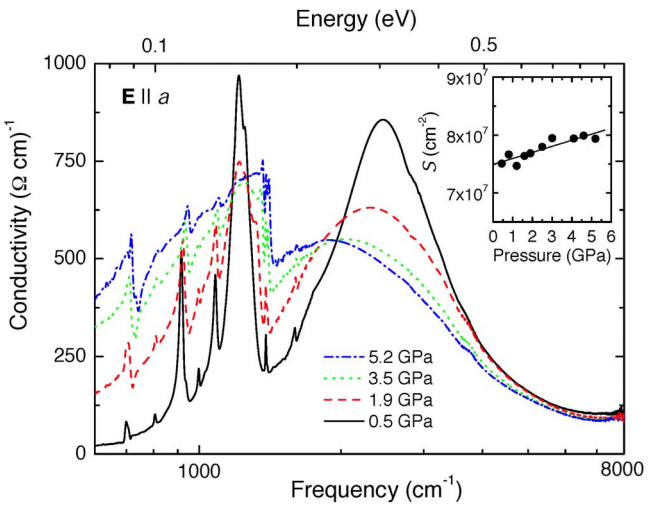

FIG. 4. (Color online) Room temperature optical conductivity $\sigma_1(\omega)$ spectra of $(TMTTF)_2AsF_6$ for $\mathbf{E}\|a$ as a function of pressure obtained by the KK analysis. Inset: Pressure dependence of the spectral weight S according to Eq. (5).

$$\phi(\omega_0) = -\frac{\omega_0}{\pi} P \int_0^{+\infty} \frac{\ln R_{s\text{-}d}(\omega)}{\omega^2 - \omega_0^2} d\omega + \left[\pi - 2 \arctan \frac{\omega_\beta}{\omega_0} \right], \tag{4}$$

where ω_β is the position of the reflectivity pole on the imaginary axis in the complex frequency plane. In case of measurements on the sample-air interface, ω_β tends towards infinity and the second term vanishes. For the sample-diamond interface the second term must, however, be taken into account. The criterium for the proper value of ω_β is the agreement between the optical conductivity obtained by the KK analysis and that from the initial fit. For the illustration of the applied data analysis a comparison of these two spectra is given in Fig. 3(b) for two different pressures; obviously, the agreement between the spectra is very good. For all studied pressures the best correspondence between the optical conductivity spectra obtained by fitting and the output of the KK analysis is achieved for the parameter ω_β=4000 cm^{-1}.

The pressure-dependent optical conductivity spectra $\sigma_1(\omega)$ of $(TMTTF)_2AsF_6$ obtained by the KK analysis are presented in Fig. 4. For the lowest applied pressure (0.5 GPa) the conductivity spectrum is very similar to the published ambient-pressure data.[24] It can be viewed as a broad absorption band centered at around 2450 cm^{-1} with a fine structure of vibronic modes.[28] This mid-IR band is usually attributed to the optical transitions across the Mott-Hubbard gap.[19,20,34] According to our results, the application of pressure causes a gradual shift of the position of the band to lower frequencies, accompanied by the onset of a Drude-like conductivity.

The spectral weight S of the absorption band was estimated by integrating the optical conductivity $\sigma_1(\omega)$ up to ω_c=7000 cm^{-1}

$$S = \int_0^{\omega_c} \sigma_1(\omega) d\omega \simeq \frac{\omega_{pa}^2}{8} = \frac{\pi N e^2}{2m_a}. \tag{5}$$

Here, ω_{pa} denotes the on-chain plasma frequency, N the electron density, and m_a the electronic band mass in the a direc-

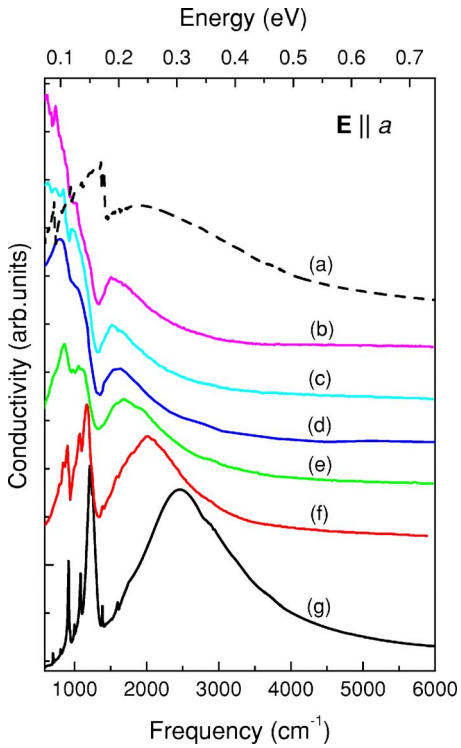

FIG. 5. (Color online) Room temperature optical conductivity $\sigma_1(\omega)$ spectra of various Bechgaard-Fabre salts for $\mathbf{E}\|a$: (a) $(TMTTF)_2AsF_6$ at 5.2 GPa; (b) $(TMTSF)_2ClO_4$; (c) $(TMTSF)_2PF_6$; (d) $(TMTSF)_2AsF_6$; (e) $(TMTTF)_2Br$; (f) $(TMTTF)_2PF_6$; and (g) $(TMTTF)_2AsF_6$ at 0.5 GPa. The spectra (b)–(f) are taken from Refs. 19 and 38.

tion. The spectral weight obtained according to Eq. (5) is almost pressure-independent (see inset of Fig. 4). The slight monotonic increase of the spectral weight (about 5% from the lowest to the highest pressure) can be attributed to the increase of the charge density due to the pressure-induced lattice compression.[35]

Based on the spectral weight, we estimated the band mass m_a of $(TMTTF)_2AsF_6$ for the lowest pressure: with a charge density of $N=1.5\times10^{21}$ cm^{-3}, as calculated from the lattice parameters,[36] we obtain a band mass $m_a\approx1.8m_e$ (m_e being the free electron mass) according to Eq. (5). This value is larger than the typical band mass in metallic TMTSF salts, where it is almost equal to the free electron mass.[34] The difference is in good agreement with the calculated values of the room temperature bandwidth for various Bechgaard-Fabre salts.[37]

In Fig. 5 the room-temperature $\mathbf{E}\|a$ optical conductivity spectra of various Bechgaard-Fabre salts[19,38] are compared with the corresponding results of the present $(TMTTF)_2AsF_6$ study at the lowest and highest applied pressure. For clarity, the curves are offset vertically and arranged from the bottom to the top with increasing chemical pressure, according to the generic phase diagram.[39] The spectrum of $(TMTTF)_2AsF_6$ at 5.2 GPa is plotted above all other spectra. Obviously, the application of *chemical* pressure shifts the strong mid-IR band to lower frequencies, suggesting the decrease of the Mott-Hubbard gap energy which is related to decrease of the stack dimerization and the strength of electronic repulsion.[20,40] As demonstrated in Figs. 4 and 5, the same effects are also induced by the application of *external* pressure to $(TMTTF)_2AsF_6$. However, a more detailed comparison reveals that the above-mentioned effects induced by chemical pressure appear to be less pronounced in the case of external pressure: even at a relatively high pressure of 5.2 GPa the on-chain optical conductivity of $(TMTTF)_2AsF_6$ differs from the ambient-pressure spectrum of $(TMTSF)_2AsF_6$; it rather resembles that of $(TMTTF)_2Br$. Thus the spectral weight of the *on-chain* optical conductivity strongly depends on the type of cation (TMTSF or TMTTF), while external pressure mainly changes the *interchain* coupling and the energy of the Mott-Hubbard gap. This issue will be further discussed in Sec. IV B.

A measure of the strength of the electronic interaction can be obtained by an analysis of the shape of the mid-IR band, i.e., the optical transitions across the Mott-Hubbard gap.[19,34] The optical conductivity well above the Mott-Hubbard gap of a 1D insulator is expected to follow a power-law decay according to[3,41,42]

$$\sigma_1(\omega)\sim\omega^{-\gamma}=\omega^{4z^2K_\rho-5}, \tag{6}$$

where $z=2$ is the order of commensurability and K_ρ is the LL exponent characterizing the strength of electronic interaction. $K_\rho=1$ corresponds to noninteracting electrons, $K_\rho<1$ to repulsive, and $K_\rho>1$ to attractive interaction between the electrons. Based on the analysis of the low-temperature optical conductivity of several TMTSF compounds, the power-law exponent γ was determined to be $\gamma\simeq1.3$, which corresponds to $K_\rho=0.23$.[19] Since the studied energy range is significantly higher than the thermal energy ($\hbar\omega\gg k_BT$), Eq. (6) should be valid also for the room-temperature optical conductivity. An analysis of the corresponding spectra in Ref. 19 gives $\gamma=1.8-2.0$ ($K_\rho=0.19-0.20$). This room-temperature value of K_ρ is only slightly smaller than the low-temperature value, indicating the weak influence of temperature on the electronic correlations in the Bechgaard-Fabre salts.

We applied Eq. (6) to the analysis of our optical conductivity spectra of $(TMTTF)_2AsF_6$. At ambient pressure we calculate $\gamma=2.85$ ($K_\rho=0.13$), in agreement with the value obtained by fitting the published spectra of $(TMTTF)_2PF_6$ and $(TMTTF)_2Br$ (3.0 and 2.5, respectively).[38] This demonstrates the reliability of our analysis. The pressure-induced change of the power-law exponent is illustrated in Fig. 6, where the measured conductivity spectra are plotted in double-logarithmic scale. One can clearly observe a gradual decrease of the slope with increase of pressure. The inset of Fig. 6 shows the power-law exponent γ and the respective value of K_ρ as a function of pressure. At 5.2 GPa we obtain $\gamma\simeq2$ and $K_\rho=0.19$ for $(TMTTF)_2AsF_6$, i.e., the typical value for TMTSF compounds. Obviously, the application of external pressure leads to a gradual decrease of the effective repulsive interaction strength in the studied compound as it was generally claimed in the earlier work.[19] Since K_ρ is close to the value 0.25 at which quarter-filling umklapp scattering is irrelevant, this means that making the system less interacting decreases strongly the Mott gap as it was observed in the previous study.[13] This could explain the large variation of the

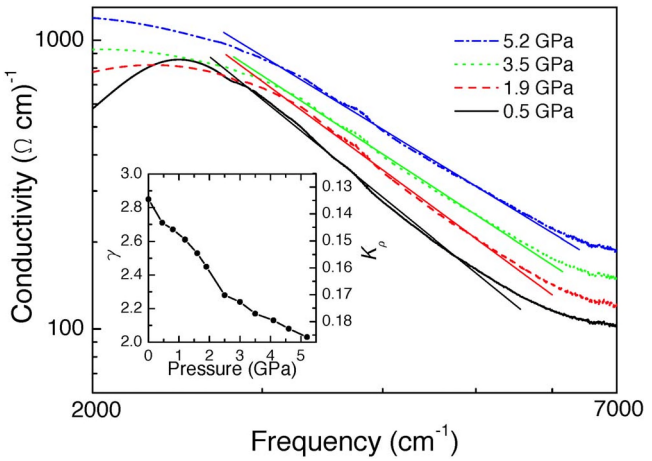

FIG. 6. (Color online) The log-log scale plot of the optical conductivity spectra $\sigma_1(\omega)$ of $(TMTTF)_2AsF_6$ for $\mathbf{E}\|a$ at different pressures. The straight lines are fits according to Eq. (6). Inset: Power-law exponent γ and corresponding LL exponent K_ρ as a function of applied pressure.

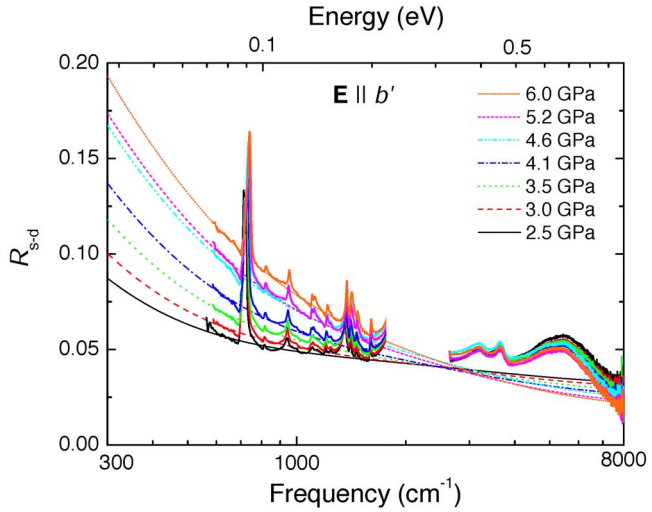

FIG. 7. (Color online) Room temperature reflectivity spectra $R_{s\text{-}d}$ of $(TMTTF)_2AsF_6$ for $\mathbf{E}\|b'$ together with the Drude fit according to Eq. (7).

Mott gap with pressure assuming that the quarter-filled umklapp process dominates. Thus, in principle, the effect of the half-filled umklapp due to the stack dimerization is not necessary in order to explain the electronic behavior in the Bechgaard-Fabre salts, although its influence cannot be completely excluded.

Furthermore, the interchain hopping is enhanced as the distance between the chains is reduced by external pressure. This effect can be best followed in the transverse optical response as discussed in the next section.

B. Transverse optical response

In the reflectivity spectrum for $\mathbf{E}\|c^*$, i.e., along the direction perpendicular to a-b plane, no pronounced electronic excitations are found in the whole studied energy range. This indicates an insulating behavior similar to the c^* axis optical conductivity in $(TMTSF)_2ClO_4$.[43] The application of pressure up to 5.8 GPa does not induce any appreciable change in the reflectivity spectra.

The optical response along the b' direction, i.e., perpendicular to the stacks of TMTTF molecules, shows a pronounced pressure-induced increase of the low-frequency reflectivity for pressures above 2 GPa. This increase signals the onset of a Drude-like contribution and thus the deconfinement of the charge carriers. The Drude-like response can be described quantitatively by estimating the transfer integral in the b' direction. For this purpose, we fitted the low-frequency part of the measured $R_{s\text{-}d}$ spectra for pressures above 2 GPa with a simple Drude model, where the dielectric function is described by

$$\epsilon(\omega) = \epsilon_\infty - \frac{\omega_p^2}{\omega(\omega + i\Gamma)}, \tag{7}$$

with ϵ_∞ being the background dielectric constant, ω_p the plasma frequency, and the optical scattering rate Γ. Γ was considered to be pressure-independent, since at room temperature it is mostly determined by the scattering on thermal phonons. Its value $\Gamma \simeq 3800\ \mathrm{cm}^{-1}$ agrees with literature data on $(TMTSF)_2PF_6$.[23,28] The measured reflectivity spectra of $(TMTTF)_2AsF_6$ together with the fits are shown in Fig. 7. The parameters of the fits and the related dc conductivity, $\sigma_{dc} = \epsilon_0 \omega_p^2 / \Gamma$, where ϵ_0 is the vacuum dielectric constant, are listed in Table I.

With the obtained values of ω_p we can calculate the interchain transfer integral t_b according to

$$t_b^2 = \frac{\pi \epsilon_0 \hbar^2 V_c t_a \omega_p^2}{4e^2 b^2}, \tag{8}$$

valid for an open Fermi surface.[44] Here V_c denotes the unit cell volume, t_a the transfer integral along the stacks, and b the interstack separation. In a simple tight-binding model t_a should scale inversely proportional to the effective mass. From the analysis of the spectral weight given in Sec. IV A, we found an effective mass $m_a = 1.8 m_e$ which is almost pressure-independent. For Bechgaard salts like $(TMTSF)_2PF_6$, which have an effective mass equal to the free electron mass, t_a is approximately 0.25 eV.[28,37] Therefore we estimated the transfer integral to be $t_a = 0.25/1.8 = 0.14$ eV for $(TMTTF)_2AsF_6$ at all pressures. Due to the lack of high-pressure structural data on $(TMTTF)_2AsF_6$, we had to make several assumptions in order to obtain b and V_c as a function of pressure: The parameter b was assumed to be linearly pressure-dependent in the whole studied pressure range, with the pressure coefficient 2.2% GPa^{-1} taken from the data of Gallois *et al.*[35] of $(TMTSF)_2PF_6$ for pressures up to 1.6 GPa. The unit cell volume V_c above 2 GPa was estimated from the pressure-induced change of the background dielectric constant $\epsilon_\infty(P)$ according to the Clausius-Mossotti relation[45]

$$\frac{\epsilon_\infty(P) - 1}{\epsilon_\infty(P) + 2} = \frac{\alpha_b}{3\epsilon_0 V_c(P)}, \tag{9}$$

where α_b is the electronic polarizability of the $(TMTTF)_2AsF_6$ unit cell in the b' direction. The value of α_b

TABLE I. Parameters obtained from the fit of the $\mathbf{E}\|b'$ reflectivity spectra of $(TMTTF)_2AsF_6$ with the Drude model according to Eq. (7): background dielectric constant ϵ_∞, plasma frequency ω_p, and dc conductivity $\sigma_{dc}=\epsilon_0\omega_p^2/\Gamma$. Also listed are the auxiliary parameters (unit cell volume V_c and carrier concentration n) and the interchain transfer integral t_b calculated according to Eq. (8).

p (GPa)	ϵ_∞	$\omega_p/2\pi c$ (cm^{-1})	σ_{dc} (Ω^{-1} cm^{-1})	V_c (Å^3)	n (10^{21} cm^{-3})	t_b (meV)
2.5	2.80	2470	26.7	560.5	1.78	25
3.0	2.87	2710	32.1	541.1	1.85	27
3.5	2.96	3000	39.5	523.9	1.91	30
4.1	3.06	3300	47.6	506.1	1.98	33
4.6	3.15	3730	61.0	493.6	2.03	37
5.2	3.25	3840	64.5	481.3	2.08	38
6.0	3.33	4120	74.3	469.6	2.13	41

was chosen to fit the known unit cell volume at pressures below 1.6 GPa[35,36] and was assumed to be pressure-independent. The carrier density was calculated assuming one carrier per unit cell. The resulting values of the unit cell volume are listed in Table I. We verified that the variation of the lattice parameters affects the calculated charge transfer integral only very weakly compared to the uncertainties of the Drude fit.

The pressure dependence of the transfer integral t_b calculated according to Eq. (8) is shown in Fig. 8. Above 2.0 GPa, t_b increases approximately linearly with increasing pressure, with a linear pressure coefficient of ≈ 5 meV/GPa. At a pressure of 4.5 GPa the value of the transfer integral in $(TMTTF)_2AsF_6$ becomes equal to the ambient-pressure value in $(TMTSF)_2PF_6$ ($t_b=35$ meV).[23,44] According to the generic temperature-pressure phase diagram of the Bechgaard-Fabre salts[39] the separation on the pressure scale between $(TMTTF)_2AsF_6$ and $(TMTSF)_2PF_6$ is about 3 GPa, i.e., appreciably smaller than 4.5 GPa. Probably, the reason for this discrepancy is the way in which the generic phase diagram was obtained. The various Bechgaard-Fabre salts are arranged in the diagram mostly according to their ground states (spin-Peierls, superconducting, etc.), whose nature is not determined solely by interchain coupling. Therefore one would not expect a perfect agreement with our room-temperature results related to the equivalence of t_b values.

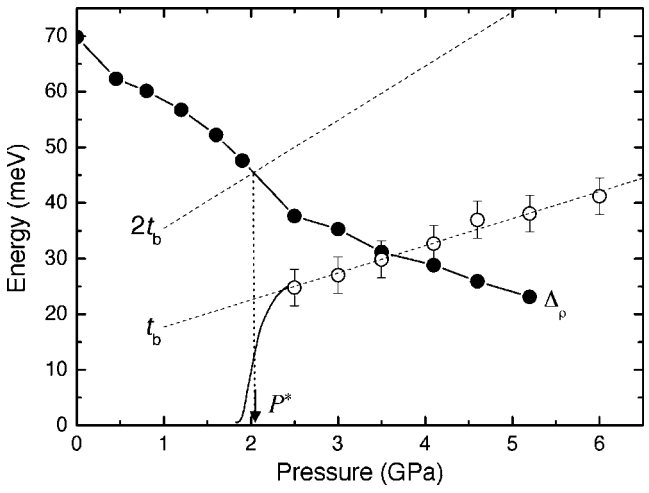

FIG. 8. Calculated interchain transfer integral t_b (open circles) and the charge gap Δ_ρ (closed circles) as a function of pressure for $(TMTTF)_2AsF_6$. The dashed lines are the linear fits of t_b and $2t_b$. P^* is the pressure at which the deconfinement transition takes place. The full line schematically shows the vanishing of t_b at the transition pressure.

With increasing pressure the deconfinement transition (trajectory 2 in Fig. 1) is expected to occur when the Mott-Hubbard gap Δ_ρ equals approximately $2t_b$.[5,13] In order to verify this condition, we estimate the pressure dependence of the charge gap Δ_ρ using the expression for a 1D quarter-filled Mott-Hubbard insulator[16,19]

$$2\Delta_\rho = W\left(\frac{g_U}{W}\right)^{1/(2-8K_\rho)}, \tag{10}$$

where $W\simeq 4t_a$ is the bandwidth and g_U the coupling constant of the corresponding umklapp process. The pressure dependence of K_ρ was obtained from the analysis of the longitudinal optical response (see Sec. IV A). As already discussed, our experiment indicates that the bandwidth W does not strongly depend on pressure and amounts to 560 meV. Using the value of $\Delta_\rho\simeq 70$ meV known from dc resistivity measurements,[46,47] the umklapp coupling constant at ambient pressure can be calculated according to Eq. (10) and amounts to $g_U=155$ meV. Since the increase of K_ρ with increasing pressure (see inset in Fig. 6) indicates a decrease of the electronic interaction, g_U should decrease as well. The functional relation between g_U and K_ρ is, however, not known for the case of a strong nonlocal electron repulsion when $K_\rho<0.5$. Therefore we calculated the pressure-dependent charge gap Δ_ρ assuming that all parameters in Eq. (10) except K_ρ are pressure-independent.

The resulting values of Δ_ρ as a function of pressure are depicted in Fig. 8. Accordingly, for $(TMTTF)_2AsF_6$ the deconfinement transition occurs at $P^*=2$ GPa. At the same time, the interchain transfer integral t_b related to single-particle hopping should renormalize to zero in the confined state.[5,7] This is directly confirmed by our experimental results: The Drude-like behavior is not observed below 2 GPa indicating a strong suppression of the interchain charge transfer, as illustrated by the full line in Fig. 8.

According to the temperature-pressure phase diagram, which is based on pressure-dependent resistivity measurements on the closely related $(TMTTF)_2PF_6$ compound,[22] the deconfinement transition occurs at a pressure of 1 GPa at room temperature. This value is somewhat lower than the pressure of the deconfinement transition in $(TMTTF)_2AsF_6$ obtained in the present study. Possibly, this discrepancy is related to the criteria which were used to specify the transition: In the mentioned work of Moser *et al.*[22] the deconfinement transition was identified based on the resistivity behavior along the a axis, whereas in the present work we refer to the onset of the charge transport along the b' direction.

The dimensional crossover (trajectory 3 in Fig. 1) is expected to reveal itself as an onset of a sharp plasma edge[23] in the b' direction, i.e., the plasma frequency ω_p should become significantly larger than the scattering rate Γ (≈ 3800 cm^{-1}). According to the values of ω_p given in Table I, the Drude response is overdamped (i.e., $\omega_p < 2\Gamma$) in the whole studied pressure range. Thus even at 6 GPa $(TMTTF)_2AsF_6$ is presumably in a 1D LL state, and the dimensional crossover is expected to occur only at even higher pressure. According to the linear extrapolation (not shown) of the pressure dependence of ω_p (which is proportional to t_b) the condition $\omega_p = 2\Gamma$ for the dimensional crossover is fulfilled at a pressure of $P_{cr} = 12.8$ GPa. The estimated value of the interchain transfer integral at this pressure is $t_b^{cr} \approx 75$ meV.

The so-obtained value of P_{cr} does not agree with the results of dc resistivity measurements along c^* published by Moser *et al.*[22] There, a strong increase of the dimensional crossover temperature T_{cr} with application of pressure was demonstrated, such that T_{cr} should reach room temperature at 3 GPa for $(TMTTF)_2PF_6$ and at 1 GPa for $(TMTSF)_2PF_6$. The former value is smaller by a factor of about 4 compared to our estimation based on the criterium of the underdamped Drude response. Therefore we suggest that this criterium should not be used for the precise determination of the dimensional crossover pressure or temperature. Rather, the observation of a well-underdamped Drude response ($\omega_p \gg 2\Gamma$) could be taken as a criterium that the system can no longer be considered as one-dimensional.

V. CONCLUSIONS

In summary, we studied the mid-IR reflectivity of $(TMTTF)_2AsF_6$ at room temperature with the incident radiation polarized along the a, b', and c^* direction as a function of quasihydrostatic pressure.

The pressure dependence of the optical conductivity along the molecular stacks ($\mathbf{E} \| a$) demonstrates a gradual onset of a Drude-like response accompanied by a decrease of the charge gap with increasing pressure. We found the band mass along the stacks $m_b = 1.8 m_e$ to be weakly pressure-dependent. Assuming that the 1D Hubbard model describes the properties of $(TMTTF)_2AsF_6$ correctly in the high-energy limit (i.e., above 2500 cm^{-1}), where the optical conductivity decays according to a power law $\sigma_1(\omega) \sim \omega^{-\gamma}$, we found the exponent γ to decrease from 2.9 at ambient pressure to 2.0 at 5.2 GPa. The corresponding LL exponent K_ρ increases from 0.13 to 0.19 indicating a weakening of the electronic interaction.

Perpendicular to the stacks the onset of an overdamped Drude-like optical conductivity is observed above 2.5 GPa for $\mathbf{E} \| b'$. The analysis of the data suggests a linear pressure-induced change of the interchain transfer integral t_b. The absence of a noticeable Drude component below $P^* \approx 2$ GPa and its appearance above this pressure is interpreted in terms of a pressure-induced deconfinement transition at P^*. For this pressure value the interchain transfer integral t_b is approximately equal to half the charge gap energy Δ_ρ. For $\mathbf{E} \| c^*$ $(TMTTF)_2AsF_6$ remains insulating up to the highest applied pressure.

ACKNOWLEDGMENTS

We thank G. Untereiner for crystal growth, as well as M. Dumm and T. Giamarchi for discussions and comments. Financial support by the DFG (Emmy Noether program) is acknowledged.

*Present address: Experimentalphysik II, Institut für Physik, Universität Augsburg, D-86135 Augsburg, Germany.
†Electronic address: christine.kuntscher@physik.uni-augsburg.de

[1] H. J. Schulz, Int. J. Mod. Phys. B **5**, 57 (1991).
[2] J. Voit, Rep. Prog. Phys. **57**, 977 (1994).
[3] T. Giamarchi, Chem. Rev. (Washington, D.C.) **104**, 5037 (2004).
[4] T. Giamarchi, Physica B **230-232**, 975 (1997).
[5] Y. Suzumura, M. Tsuchiizu, and G. Grüner, Phys. Rev. B **57**, R15040 (1998).
[6] M. Tsuchiizu, Y. Suzumura, and T. Giamarchi, Prog. Theor. Phys. **101**, 763 (1999).
[7] M. Tsuchiizu and Y. Suzumura, Phys. Rev. B **59**, 12326 (1999).
[8] K. Le Hur, Phys. Rev. B **63**, 165110 (2001).
[9] S. Biermann, A. Georges, A. Lichtenstein, and T. Giamarchi, Phys. Rev. Lett. **87**, 276405 (2001).
[10] M. Tsuchiizu, P. Donohue, Y. Suzumura, and T. Giamarchi, Eur. Phys. J. B **19**, 185 (2001).
[11] In principle, an effective interchain hopping $t_\perp^{\text{eff}}$ needs to be taken into account, since the interchain interaction leads to a renormalization.
[12] C. Berthod, T. Giamarchi, S. Biermann, and A. Georges, cond-mat/0602304 (to be published).
[13] V. Vescoli, L. Degiorgi, W. Henderson, G. Grüner, K. P. Starkey, and L. K. Montgomery, Science **281**, 1181 (1998).
[14] D. Jérome and H. J. Schulz, Adv. Phys. **31**, 299 (1982).
[15] T. Ishiguro, K. Yamaji, and G. Saito, *Organic Superconductors* (Springer, Berlin, 1998).
[16] D. Jerome, Chem. Rev. (Washington, D.C.) **104**, 5565 (2004).
[17] F. Zamborszky, W. Yu, W. Raas, S. E. Brown, B. Alavi, C. A. Merlic, and A. Baur, Phys. Rev. B **66**, 081103(R) (2002).
[18] F. Nad, P. Monceau, C. Carcel, and J. M. Fabre, Phys. Rev. B **62**, 1753 (2000); D. S. Chow, F. Zamborszky, B. Alavi, D. J. Tan-

tillo, A. Baur, C. A. Merlic, and S. E. Brown, Phys. Rev. Lett. **85**, 1698 (2000); P. Monceau, F. Y. Nad, and S. Brazovskii, *ibid.* **86**, 4080 (2001).
[19] A. Schwartz, M. Dressel, G. Grüner, V. Vescoli, L. Degiorgi, and T. Giamarchi, Phys. Rev. B **58**, 1261 (1998).
[20] J. Favand and F. Mila, Phys. Rev. B **54**, 10425 (1996).
[21] V. Vescoli, L. Degiorgi, K. P. Starkey, and L. K. Montgomery, Solid State Commun. **111**, 507 (1999).
[22] J. Moser, M. Gabay, P. Auban-Senzier, D. Jérome, K. Bechgaard, and J. M. Fabre, Eur. Phys. J. B **1**, 39 (1998).
[23] C. S. Jacobsen, D. B. Tanner, and K. Bechgaard, Phys. Rev. Lett. **46**, 1142 (1981).
[24] M. Dumm, B. Salameh, M. Abaker, L. Montgomery, and M. Dressel, J. Phys. IV **114**, 57 (2004).
[25] H. K. Mao, J. Xu, and P. M. Bell, J. Geophys. Res., [Oceans] **91**, 4673 (1986).
[26] *Handbook of Optical Constants of Solids*, edited by E. D. Palik (Academic Press, London, 1998).
[27] M. I. Eremets and Y. A. Timofeev, Rev. Sci. Instrum. **63**, 3123 (1992).
[28] C. S. Jacobsen, D. B. Tanner, and K. Bechgaard, Phys. Rev. B **28**, 7019 (1983).
[29] G. M. Begun and A. C. Rutenberg, Inorg. Chem. **6**, 2212 (1967).
[30] M. Meneghetti, R. Bozio, I. Zanon, C. Pelice, C. Ricotta, and M. Zanetti, J. Chem. Phys. **80**, 6210 (1984).
[31] J. S. Plaskett and P. N. Schatz, J. Chem. Phys. **38**, 612 (1963).
[32] F. Gervais, *Infrared and Millimetre Waves*, Vol. 8 (Academic Press, New York, 1983).
[33] R. D. McDonald, Ph.D. thesis, Magdalen College, Oxford, 2001.
[34] M. Dressel, A. Schwartz, G. Grüner, and L. Degiorgi, Phys. Rev. Lett. **77**, 398 (1996).
[35] B. Gallois, J. Gaultier, T. Lamcharfi, F. Bechtel, A. Filhol, L. Ducasse, and M. Abderrabba, Synth. Met. **19**, 321 (1987).
[36] R. Laversanne, C. Coulon, B. Gallois, J. P. Pouget, and R. Moret, J. Phys. (France) Lett. **45**, L393 (1984).
[37] L. Ducasse, M. Abderrabba, J. Hoarau, M. Pesquer, B. Gallois, and J. Gaultier, J. Phys. C **19**, 3805 (1986).
[38] D. Pedron, R. Bozio, M. Meneghetti, and C. Pecile, Phys. Rev. B **49**, 10893 (1994).
[39] C. Bourbonnais and D. Jérome, Science **281**, 1155 (1998).
[40] K. Penc and F. Mila, Phys. Rev. B **50**, 11429 (1994).
[41] T. Giamarchi, Phys. Rev. B **44**, 2905 (1991).
[42] D. Controzzi, F. H. L. Essler, and A. M. Tsvelik, Phys. Rev. Lett. **86**, 680 (2001).
[43] W. Henderson, V. Vescoli, P. Tran, L. Degiorgi, and G. Grüner, Eur. Phys. J. B **11**, 365 (1999).
[44] J. F. Kwak, Phys. Rev. B **26**, 4789 (1982).
[45] N. Ashcroft and N. Mermin, *Solid State Physics* (Saunders College, Philadelphia, 1976).
[46] C. Coulon, P. Delhaes, S. Flandrois, R. Lagnier, E. Bonjour, and J. M. Fabre, J. Phys. (France) **43**, 1059 (1982).
[47] M. Dressel, P. Hesse, S. Kirchner, G. Untereiner, M. Dumm, J. Hemberger, A. Loidl, and L. Montgomery, Synth. Met. **120**, 719 (2001).